AIAA JOURNAL
Vol. 45, No. 2, February 2007

Wavelength-Scanned Tunable Diode Laser Temperature Measurements in a Model Gas Turbine Combustor

Xin Zhou,* Jay B. Jeffries,† and Ronald K. Hanson‡
Stanford University, Stanford, California 94305
and
Guoqiang Li§ and Ephraim J. Gutmark¶
University of Cincinnati, Cincinnati, Ohio 45221

DOI: 10.2514/1.26624

Two tunable diode laser temperature sensors are compared for nonintrusive determination of gas temperature and temperature fluctuations in a swirl-stabilized atmospheric-pressure flame. Time-resolved temperature is inferred from the ratio of integrated absorbance of two selected H_2O transitions observed by scanning the wavelength of a single diode laser. The first sensor uses direct absorption near 1.8 μm, and the second sensor uses wavelength-modulation spectroscopy with second-harmonic detection (WMS-2f) near 1.4 μm. Both sensors are based on the single-laser concept, which can make the system compact, rugged, low-cost, and simple to operate. The scanned-wavelength approach can minimize interference from emission and provide robust absorption measurements. Time-resolved and real-time (no postprocessing) temperature measurements are presented for both liquid and gaseous fuels, and a systematic comparison of the performance of the two sensors is reported. We find the two-line absorption ratio to have excellent potential as a temperature-based control variable for these swirl-stabilized flames.

Nomenclature

A	=	modulation amplitude, cm^{-1}
A_j	=	integrated absorbance of the jth transition
f	=	modulation frequency, Hz
H_n	=	Fourier harmonic function
$I(\nu)$	=	laser intensity
$I_0(\nu)$	=	baseline laser intensity without absorption
L	=	laser path length through absorbing medium, cm
P	=	gas pressure, atm
R	=	ratio of integrated absorbance, $f(T)$
$S(T, \nu)$	=	temperature-dependent line strength, cm^{-2}/atm
T	=	gas temperature, K
X_i	=	mole fraction of species i
α	=	absorbance
ν	=	laser frequency, cm^{-1}
τ_ν	=	fractional transmission at frequency ν
ϕ_ν	=	normalized line-shape function, cm

I. Introduction

TUNABLE diode laser (TDL) sensors are useful diagnostic tools for propulsion and combustion applications, providing time-resolved measurements of gas temperature, species concentration, and gas velocity, as well as mass and momentum flux [1]. Water vapor (H_2O) is an ideal species to monitor, because it is naturally present in air, it is one of the primary products of hydrocarbon combustion, and it absorbs strongly throughout the near-infrared region. Two-line thermometry based on high-resolution-absorption spectroscopy of H_2O has been developed and demonstrated in a variety of reactive environments. For example, Furlong et al. [2] successfully demonstrated a multiplexed TDL sensor using two H_2O transitions near 1.34 and 1.39 μm for combustion control of an acoustically forced dump combustor; Ebert et al. [3,4] measured gas temperature in large-scale gas- and coal-fired combustion systems using water transitions near 812 nm; Sanders et al. [5] measured gas temperature in pulse detonation engines using water transitions near 1.4 μm; and Rieker et al. [6] and Mattison et al. [7] used similar transitions for temperature during the compression stroke of an internal-combustion (IC) engine. Liu et al. [8] developed and applied scanned-wavelength direct absorption of water vapor near 1.4 μm to monitor temperature at kilohertz rates in a model scramjet combustor.

However, these previous TDL temperature sensors used a wavelength-multiplexing scheme that required multiple lasers. If transitions can be selected close enough together to be covered with the small cm^{-1} scan range of a typical TDL, the complexity of the wavelength-multiplexed scheme can be avoided. A few single-laser TDL temperature sensors have been reported previously, based on fortuitous coincidences of diode laser wavelengths and water transitions; for example, Arroyo and Hanson [9] identified a useful H_2O line pair near 1.38 μm for single-laser H_2O thermometry, and more recently, Gharavi and Buckley [10] investigated a H_2O line pair near 1.48 μm for temperature measurements. In recent work, we have used a design-rule-based strategy to systematically evaluate and optimize the selection of H_2O vapor transitions from the vast number of possibilities in the region of 1–2 μm [11–13]. This work has led to two single-TDL temperature sensors, one using direct absorption near 1.8 μm [11] and the other using scanned-wavelength-modulation spectroscopy with second-harmonic detection (scanned WMS-2f) near 1.4 μm [12]. For each of these sensors, the logic of the line-selection process was discussed in detail, the fundamental spectroscopic data for the selected lines were carefully measured in a heated cell, and the performance was validated in a controlled laboratory environment [11,12].

This paper presents a systematic comparison of the performance of Stanford's direct-absorption temperature sensor near 1.8 μm and the

Received 18 July 2006; accepted for publication 24 October 2006.

*Graduate Research Assistant, Mechanical Engineering, currently Spectra Sensors, Inc., 972 North Amelia Avenue, San Dimas, CA 91773.
†Senior Research Associate, Mechanical Engineering. Associate Fellow AIAA.
‡Professor, Mechanical Engineering. Fellow AIAA.
§Research Assistant Professor. Member AIAA.
¶Professor. Associate Fellow AIAA.

scanned-WMS-2f temperature sensor near 1.4 μm, using measurements in a swirl-stabilized, atmospheric-pressure combustor at the University of Cincinnati; a preliminary report of these measurements was presented at the 43rd AIAA Aerospace Sciences Meeting and Exhibit in 2005 [14]. To our knowledge, this work presents the first TDL thermometry in a liquid-fueled, swirl-stabilized spray flame. The performance differences between the scanned WMS-2f and wavelength-scanned direct absorption are discussed in detail. The use of line selection to minimize ambient interference is illustrated. The measurements demonstrate the ability of TDL temperature sensing to monitor temperature fluctuations in harsh, practical environments and, thus, illustrate the potential of TDL sensors to provide a temperature-based control variable.

II. Absorption Spectroscopy Fundamentals

The sensor design and operation of the 1.8-μm time-resolved and the 1.4-μm real-time temperature sensors are detailed in [11,12], respectively. Here, we present only the design information needed to compare direct absorption and WMS-2f sensor strategies.

A. Direct-Absorption Temperature Sensor

The fractional transmission of monochromatic laser light along a uniform path is described by the Beer–Lambert relation:

$$\tau_\nu = \left(\frac{I(\nu)}{I_o(\nu)}\right) = \exp[-P \cdot X_i \cdot S(T, \nu_j) \cdot \phi_\nu \cdot L] = \exp(-\alpha_\nu) \quad (1)$$

where $I(\nu)$ and $I_0(\nu)$ are transmitted and incident, respectively; $S(T, \nu_j)$ [cm^{-2} atm^{-1}] is of the jth transition centered at ν_j [cm^{-1}]; and ϕ_ν [cm] for the particular transition probed is normalized such that $\int \phi(\nu)\,\mathrm{d}\nu \equiv 1$. The combined quantity $\alpha_\nu = P \cdot X_i \cdot S(T, \nu_j) \cdot \phi_\nu \cdot L$ is known as the absorbance, and the integrated absorbance for the jth transition is $A_j \equiv \int \alpha_\nu\,\mathrm{d}\nu$.

The temperature can be inferred from the measured ratio of integrated absorbance for two different temperature-dependent transitions (illustrated in Fig. 1). Because the two integrated absorbance values are obtained with the same partial pressure of water and same path length, the ratio of these two integrals reduces simply to the ratio of line strengths:

$$R = \frac{A_1}{A_2} = \frac{\int PX_i S_1(T, \nu_1)\phi_\nu L\,\mathrm{d}\nu}{\int PX_i S_2(T, \nu_2)\phi_\nu L\,\mathrm{d}\nu} = \frac{S_1(T, \nu_1)}{S_2(T, \nu_2)} = \frac{S(T_0, \nu_1)}{S(T_0, \nu_2)} \exp\left[-\left(\frac{hc}{k}\right)(E_1'' - E_2'')\left(\frac{1}{T} - \frac{1}{T_0}\right)\right] \quad (2)$$

where the reference temperature is T_0 [K], and E_j'' is the lower-state energy of the jth transition [cm^{-1}].

B. Scanned WMS-2f Temperature Sensor

For scanned-wavelength-modulation absorption spectroscopy, the laser is driven by a combination of a slow ramp and a fast sinusoidal modulation, and the laser output frequency can be expressed by

$$\nu(t) = \overline{\nu(t)} + a\cos(2\pi f t) \quad (3)$$

where $\overline{\nu(t)}$ [cm^{-1}] is the center frequency of the modulation and varies slowly in time, and a [cm^{-1}] is the modulation amplitude. Following [15–18], the quantity τ can be expanded in a Fourier cosine series:

$$\tau[\overline{\nu(t)} + a\cos(2\pi f t)] = \sum_{n=0}^{+\infty} H_n[\overline{\nu(t)}, a]\cos(2\pi n f t) \quad (4)$$

where $H_n[\overline{\nu(t)}, a]$ is the nth Fourier coefficient of the transmission coefficient [16]:

$$H_0[\overline{\nu(t)}, a] = \frac{1}{2\pi}\int_{-\pi}^{\pi} \tau[\overline{\nu(t)} + a\cos\theta]\,\mathrm{d}\theta \quad (5)$$

$$H_n[\overline{\nu(t)}, a] = \frac{1}{\pi}\int_{-\pi}^{\pi} \tau[\overline{\nu(t)} + a\cos\theta]\cdot\cos(n\theta)\,\mathrm{d}\theta \quad (6)$$

Typically, the second-harmonic component of the signal is detected and, in the limit of weak absorbance (less than 0.1), this Fourier coefficient is given by

$$H_2[\overline{\nu(t)}, a] = -\frac{S \cdot P \cdot X_i \cdot L}{\pi}\int_{-\pi}^{\pi} \phi[\overline{\nu(t)} + a\cos\theta]\cdot\cos(2\theta)\,\mathrm{d}\theta \quad (7)$$

The 2f signal is proportional to $I_0 H_2(\bar{\nu}, a)$ if intensity modulation effects are neglected [16].

Similar to the direct-absorption technique, WMS-2f employs the two-line method for temperature measurements, because the 2f peak-height ratio of two transitions is a function of temperature (Fig. 2), closely related to the ratio of the absorption line strengths [17].

$$R_{2f,\mathrm{ratio}} = \frac{I_{\bar{\nu}_1}}{I_{\bar{\nu}_2}}\cdot\frac{H_2(\bar{\nu}_1)}{H_2(\bar{\nu}_2)} = \frac{I_{\bar{\nu}_1}}{I_{\bar{\nu}_2}}\cdot\frac{S_1(T)}{S_2(T)} \cdot \frac{\int_{-\pi}^{\pi}\phi[\bar{\nu}_1 + a_1\cos\theta]\cos(2\theta)\,\mathrm{d}\theta}{\int_{-\pi}^{\pi}\phi[\bar{\nu}_2 + a_2\cos\theta]\cos(2\theta)\,\mathrm{d}\theta} \quad (8)$$

where $I_{\bar{\nu}_1}$ and $I_{\bar{\nu}_2}$ are the laser intensities at line center of transitions 1 and 2, respectively, and $H_2(\bar{\nu}_1)$ and $H_2(\bar{\nu}_2)$ are the second-harmonic Fourier coefficients that are given by Eq. (7).

C. Comparison of 1.8-μm Direct-Absorption and 1.4-μm WMS-2f Temperature Sensors

The calculated spectroscopic features for the water line pairs of the 1.4- and 1.8-μm sensors are shown in Fig. 3 for temperatures of 296, 1000, and 2000 K, and the transitions are listed in Table 1. The line selection of these two sensors and the quantitative spectroscopy of the target lines and their neighbors have been discussed in detail [11,12]. Both sensors use the two-line concept, although there are additional neighboring transitions, and the 1.8-μm scan includes four lines, whereas the 1.4-μm scan includes three. For the 1.8-μm case, the target lines 1 and 2 are resolved from line 3, and line 4 has negligible absorbance for temperatures above 800 K (the lower

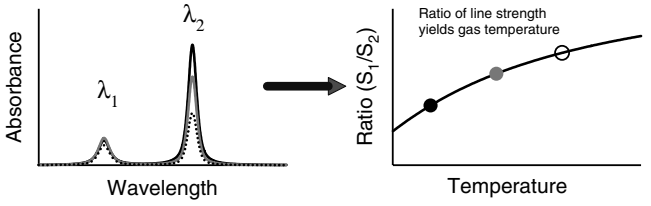

Fig. 1 Illustration of the measurement principle of the wavelength-scanned, direct-absorption 1.8-μm sensor. Measurements of two absorption features from a single-TDL scan shown for $T_{\mathrm{black}} < T_{\mathrm{gray}} < T_{\mathrm{dotted}}$; temperature is inferred from the ratio of integrated absorbance of the two different temperature-dependent transitions.

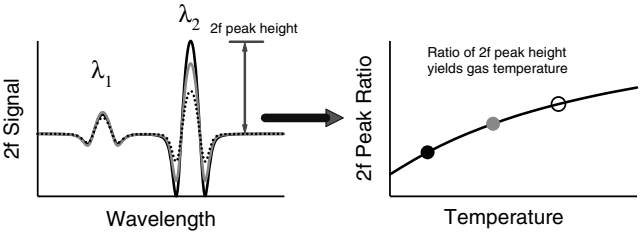

Fig. 2 Illustration of the measurement principle of the 1.4-μm sensor. WMS measurements of two absorption features from a single-TDL scan shown for $T_{\mathrm{black}} < T_{\mathrm{gray}} < T_{\mathrm{dotted}}$; temperature is inferred from the 2f peak ratio of the two different temperature-dependent transitions.

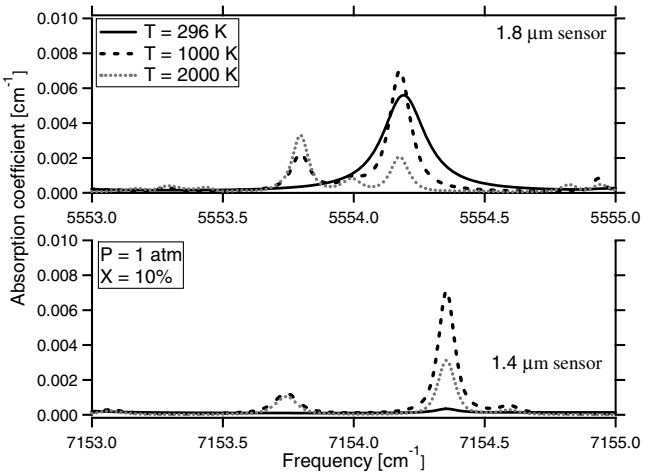

Fig. 3 Calculated spectroscopic features for water line pairs in the 1.4- and 1.8-μm sensors based on HITRAN [22]; $X_{H_2O} = 10\%$ for $T =$ 296 K (solid line), 1000 K (dashed line), and 2000 K (dotted gray line).

bound temperature for this sensor; note that at lower temperatures, the absorbance of the high E'' transition becomes too weak for a precise ratio with the absorbance of the low E'' transition). For the 1.4-μm case, the two high E'' lines are completely blended at atmospheric pressure and are considered as a single line, and the total line strength is the sum of the two contributions.

The 1.8-μm line pair is more sensitive to temperature, whereas the 1.4-μm line pair is less sensitive to interference from ambient water vapor. The lower-state energy difference ($\Delta E''$) of the 1.8-μm line pair is 2332 cm^{-1}, and the $\Delta E''$ of the 1.4-μm line pair is 764 cm^{-1}. Because the temperature sensitivity is highest for the largest difference [11,12] in $\Delta E'' = |E_1'' - E_2''|$, the temperature sensitivity of the 1.8-μm sensor is about three times better than the 1.4-μm sensor. Because the laser scan of the 1.8-μm sensor includes two low-energy transitions ($E'' \sim 983$ cm^{-1} and $E'' \sim 173$ cm^{-1}), the 1.8-μm sensor is sensitive to interference from ambient water vapor, as seen in Fig. 3, which shows the relatively large absorbance at 296 K. Thus, this sensor requires the use of nitrogen or dry air to purge the laser path outside the measurement zone to eliminate interference from ambient humidity in the air. Because the lowest energy transition in the scan of the 1.4-μm sensor has an E'' near 1789 cm^{-1}, this sensor is insensitive to interference from cold humid room air, as illustrated in Fig. 3, which shows the relatively small absorption observed at 296 K.

Data analysis of injection-current-tuned TDL direct absorption requires baseline fitting to account for the change in laser intensity as the laser frequency is tuned. Because the absorption signal is a small change in the transmitted intensity, the integrated absorbance is more precisely determined by the use of a Voigt fit to the line shape. This analysis is time-consuming and requires postprocessing for rapid (kilohertz) time resolution. By contrast, the near-zero baseline of the WMS-2f signal and its significantly larger signal-to-noise ratio (SNR), compared with direct-absorption measurements of small (less than a few percent) absorbance, enable use of the 2f peak-height ratio to infer temperature. This avoids time-consuming fits and enables real-time data analysis of the temperature fluctuations with the scanned WMS-2f sensor. In these experiments, we demonstrated a 2-kHz measurement rate (2-kHz scan repetition rate) with this approach [12].

For practical combustor applications, the use of fiber-coupled lasers and fiber components simplifies the implementation of the TDL sensor. Such fiber technology is well developed in the telecommunications wavelength region (1.3–1.65 μm), and thus the sensor at 1.4 μm has many attractive features that are superior to the free-space lasers and optics at 1.8 μm. These include advanced laser performance, simple installation, easy laser beam alignment, improved ruggedness and flexibility, and reduced overall system cost.

III. Combustion Measurements

Stanford's 1.4- and 1.8-μm TDL sensors were used for temperature measurements in an atmospheric-pressure, swirl-stabilized spray combustor [19] in the Gas Dynamics and Propulsion Laboratory at the University of Cincinnati, and a preliminary account was presented at the 43rd AIAA Aerospace Sciences Meeting and Exhibit in 2005 [14]. The inlet air is preheated for inlet temperatures up to 1400°C at an air mass flow rate up to 1700 slm (2.2 kg/ min) with a 36-kW electric heater. This inlet flow is conditioned with a series of five fine screens and a honeycomb flow straightener. A triple annular swirler (TAS) with a 5-cm diameter is centered at the dump plane and is installed on the end flange of the plenum chamber. The combustor was operated on a variety of hydrocarbon fuels, and results are presented here for gaseous propane and liquid ethanol.

Two tubular combustion chambers were used: 1) a rectangular chamber with a 100 × 100 mm cross section, 450-mm long with flat quartz windows for optical access, and 2) a round (100-mm diameter) quartz tube 470-mm long with optical access directly through the chamber walls. Exhaust gas is sampled at the combustor exit and analyzed through individual commercial gas analyzers for CO, NOx, and UHC. Both the air- and fuel-flow rates are metered, and other operating parameters, including plenum pressure, inlet air temperature, fuel temperature, combustion flame temperature, and emission data are continuously recorded by a Labview control program. Two loudspeakers were installed on the plenum chamber and can be driven by a function generator to artificially generate acoustic disturbance for the airflow.

A. Direct-Absorption Temperature Sensor Near 1.8 μm

Figure 4 illustrates the general arrangement used for the 1.8-μm sensor. The output from the distributed feedback (DFB) laser near 1.8 μm is directed across the flame on the swirl-stabilized spray combustor, using appropriate mirrors. The low-power (less than 1-mW) 1.8-μm near infrared (NIR) laser is coaligned with a visible laser (HeNe) beam to aid alignment. The diode laser is temperature- and current-controlled (ILX Lightwave LDC-3900) and injection-current tuned over the wavelength region, illustrated in Fig. 3. The beam path is purged to avoid interference from ambient water vapor. The laser beam is angled ~10 deg in the rectangular duct (horizontally) to avoid the etalon interferences from multiple reflections from the flat quartz windows. The total path length is 102 mm.

The laser is scanned at 2 kHz and the transmitted intensity is sampled at 1 MHz; an average of four scans is used to improve the

Table 1 Spectroscopic data for the 1.4- and 1.8-μm temperature sensor

Line no.	Frequency, cm^{-1}	Line strength at 296 K, cm^{-2}/atm	Lower-state energy, cm^{-1}
1.8-μmsensor			
2 (high E'')	5553.86	7.30×10^{-7}	3314.9
3	5554.04	3.63×10^{-7}	3139.5
1 (low E'')	5554.18	7.66×10^{-3}	982.9
4	5554.21	9.20×10^{-3}	173.4
1.4-μm sensor			
High E'' 1	7153.72	1.90×10^{-6}	2552.9
High E'' 2	7153.75	6.15×10^{-6}	2552.9
Low E''	7154.35	3.67×10^{-4}	1789.0

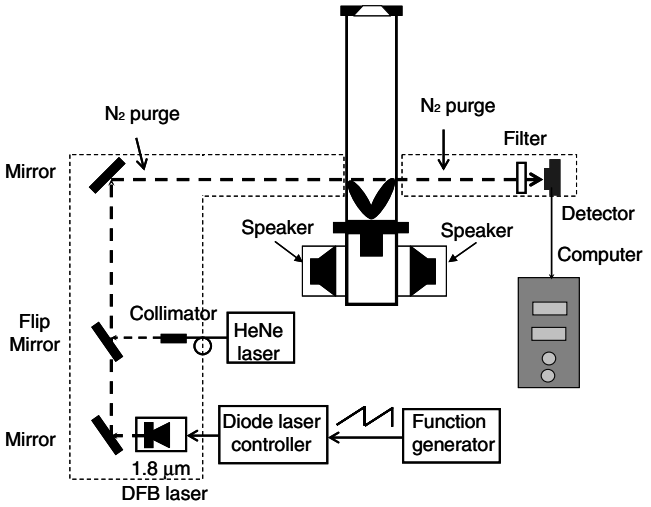

Fig. 4 Schematic diagram of the 1.8-μm temperature sensor applied to the swirl-stabilized spray combustor. Note that the flip mirror allows use of the visible HeNe beam for alignment.

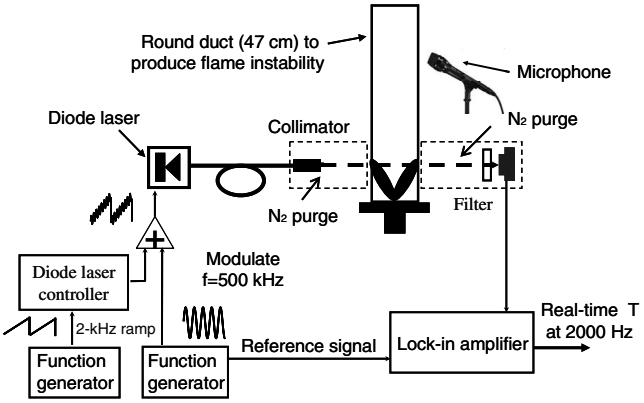

Fig. 6 Schematic diagram of the 1.4-μm temperature sensor applied to the swirl-stabilized spray combustor.

SNR, which reduces the time resolution to 500 Hz. The baseline laser intensity is determined from a polynomial fit to the transmitted intensity beyond the wings of the absorption features, and the absorbance is fit to a convolution of four Voigt absorption line shapes. Temperature is determined from the ratio of the integrated absorbance of lines 1 and 2 (Table 1) for a single axial location at 50 mm downstream of the nozzle. Figure 5 shows an example of the absorbance for gas-fueled (0.02 kg/min propane and 0.37 kg/min air) and liquid-fueled (0.1 kg/min ethanol and 2.1 kg/min air) flames. Note the SNR is reduced in liquid-fueled experiments, due to beam steering effects and unburned liquid droplet interference.

The airflow can be modulated by driving the plenum pressure with the loudspeakers that are illustrated in Fig. 4, producing a fluctuating flame stoichiometry (hence, heat-release rate). Fourier analysis of the time-resolved temperature identifies the fluctuation frequency, illustrating the potential of this sensor for fluctuation measurements. The TDL sensor has line-of-sight (LOS) spatial resolution, and the optimum position to observe these fluctuations is near the flame tip, off the centerline of the burner.

B. Scanned WMS-2f temperature Sensor Near 1.4 μm

The WMS-2f temperature sensor is illustrated in Fig. 6; the laser beam exits the optical fiber and is collimated with a lens across the flame, filtered, and detected. The wavelength of a single DFB diode laser operating near 1.4 μm is injection-current scanned with a 2-kHz sawtooth ramp, with a sinusoidal modulation at 500 kHz. The second-harmonic component of the signal from the transmitted laser intensity is isolated by a lock-in amplifier (Perkin-Elmer Model 7280) with a 1-μs time constant. The temperature is inferred from the 2f peak-height ratio, with a real-time data processing code written in C++ on a dedicated industrial PC.

The flame is confined in a round quartz duct, and the laser beam is intentionally kept away from the centerline of the round quartz duct to minimize etalon interference. Measurements were made at a radial position 15 mm from the spray centerline and an axial position 50.8 mm downstream of the nozzle exit, with a total path length of 97 mm. Figure 7 illustrates representative WMS-2f single-scan line shapes over the wavelength range illustrated in Fig. 3 for gas-fueled (0.08 kg/min propane and 1.1 kg/min air) and liquid-fueled (0.15 kg/min ethanol and 2.1 kg/min air) flames. Note that the SNR is nearly the same for liquid and gas fuels, illustrating the use of WMS to suppress the low-frequency noise that reduced the SNR of the direct-absorption sensor in liquid-fueled flames.

Figure 8 shows a half-second of time-resolved gas-temperature data in the propane/air flame. Fourier analysis of these data, also shown, identifies the natural flame instability of the swirl-flame confined in a round duct. The 2-kHz scan rate provides a time resolution of 0.5 ms and the temperature analysis provides real-time temperature with this resolution, as well as a running fast Fourier transform (FFT), using 0.5 s of temperature data. The dominant mode (232 Hz) and its first harmonic (464 Hz) are clearly revealed. Acoustic signals are simultaneously detected by a Brüel & Kjær microphone (Model 4939-A-011) located 0.5 m from the combustor

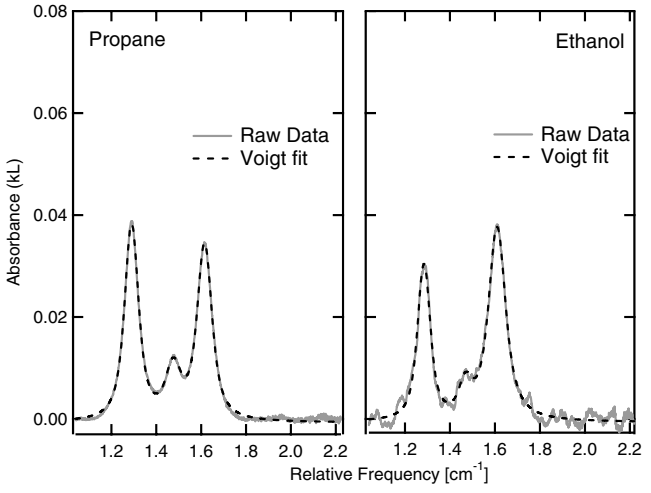

Fig. 5 Direct-absorption measurements (gray line) of H_2O vapor absorption and Voigt fits (dashed line) to the absorption line shapes with the 1.8-μm temperature sensor (average of four 2-kHz scans) recorded in swirl-stabilized flames with gaseous fuel (propane) and liquid fuel (ethanol).

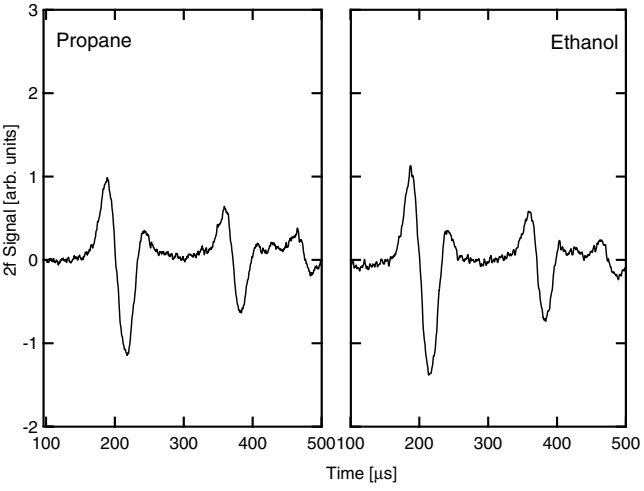

Fig. 7 Scanned WMS-2f H_2O 2f absorption (single scan at 2 kHz) recorded with the 1.4-μm temperature sensor in swirl-stabilized flames with gaseous fuel (propane) and liquid fuel (ethanol).

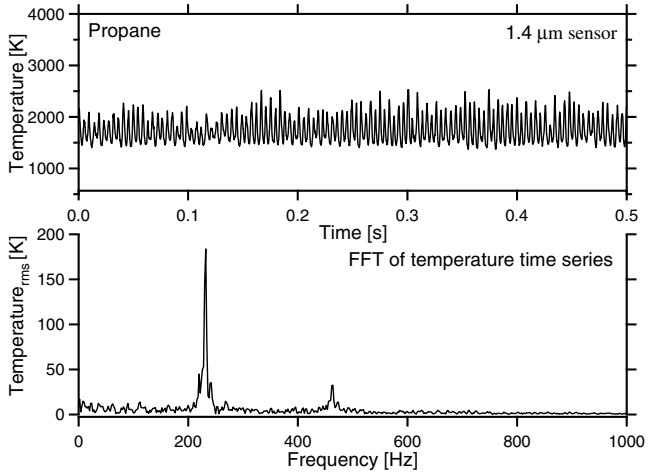

Fig. 8 Measured temperature and its power spectrum in the burned region above the propane–air flame.

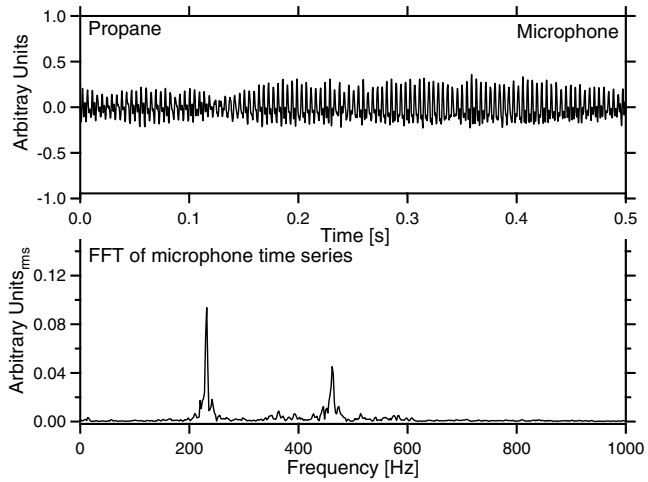

Fig. 9 Measured acoustic signal and its power spectrum in the burned region above the propane–air flame.

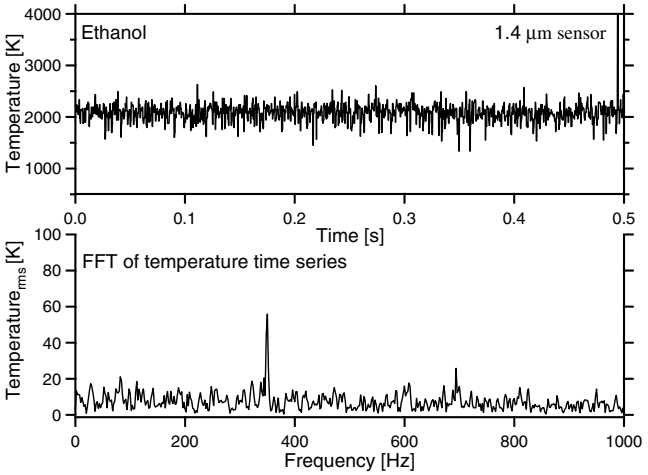

Fig. 10 Measured temperature and its power spectrum in the burned region above the ethanol–air flame.

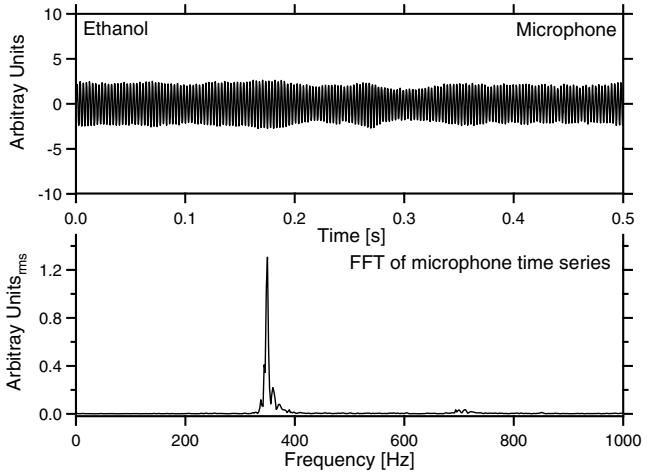

Fig. 11 Measured acoustic signal and its power spectrum in the burned region above the ethanol–air flame.

chamber, and the acoustic signal and its power spectrum, shown in Fig. 9, have a similar SNR for this flame. These results demonstrate the sensor's ability to track the temperature fluctuations, illustrating a potential application for combustion instability control.

Similar temperature measurements were made in the ethanol–air flame, as shown in Fig. 10. Here, a slightly different duct is used, and the dominant 350-Hz mode and its 700-Hz harmonic are clearly evident. Simultaneous microphone measurements are shown in Fig. 11. Although this microphone data have a higher SNR, the time limitations of this field measurement campaign did not allow us to optimize the TDL sensor for a quantitative comparison of the two sensors. For example, the TDL LOS was not varied, nor did we explore additional filters to reduce the background optical noise on the signal to the lock-in from the more robust liquid-fueled flame.

IV. Discussion

To our knowledge, we present the first TDL thermometry in a liquid-fueled, swirl-stabilized spray combustor. The TDL sensor is appealing because it is noninvasive and has a LOS spatial resolution. The TDL capability to monitor the local temperature fluctuations (hence, heat-release fluctuations) provides interesting impetus for investigation of this physics-based control sensor. A precision temperature inferred from the ratio of two absorption transitions requires a uniform distribution of temperature and gas composition along the sensor LOS. In the practical flames studied here, even though the temperature distribution is not uniform (and even though the sensor does not return a precise temperature), the temporal fluctuations of the temperature provide a measure of the flame stability. Subsequent work in our laboratory at Stanford has shown that these fluctuations provide a very robust control variable for flame stability and to suppress lean blowoff [20,21].

Although the direct-absorption 1.8-μm sensor has the capability to measure temperature of both the gas- and liquid-fueled swirling flames, several limitations are encountered:

1) Extra efforts are required for the laser alignment and nitrogen purge, due to the low power of the laser.

2) The small direct-absorption signals required averaging to obtain a sufficient SNR under noisy conditions, which limits the measurement bandwidth.

3) The lack of fiber-coupled diode lasers makes the use of this sensor less convenient.

These limitations could all be solved with laser devices at 1.8 μm, similar to the capabilities of telecommunications-grade lasers at 1.4 μm.

The 1.8-μm sensor has two additional drawbacks:

1) The strong room-temperature absorption makes the laser sensitive to cold boundary layers in the flame duct. second,

2) The use of a direct-absorption strategy increases the sensitivity to baseline noise and requires data reduction that is not easily amenable to a real-time bandwidth suitable for control applications.

The scanned WMS-2f 1.4-μm temperature sensor has several advantages over the wavelength-scanned, direct-absorption 1.8-μm temperature sensor:

1) The transitions chosen near 1.4 μm are free from interference from room-temperature ambient humidity.

2) The transitions used for the 1.4-μm sensor have larger E'' and are thus more sensitive to the hottest parts of the LOS path, improving its sensitivity to fluctuations of the high-temperature regions along the LOS.

3) The availability of fiber-coupled lasers at 1.4 μm provides an easily installed sensor.

4) The use of WMS-2f sensor architecture improves the SNR, especially in liquid-fueled flames, and enables rapid data reduction with a 2-kHz real-time bandwidth.

Recently, the scanned-WMS-2f temperature sensor has been used in our laboratory for the suppression of lean blowout [20] and flame instabilities [21] in a similar propane-fueled, swirl-stabilized combustor. This later work also optimized the TDL sensor LOS and compared the TDL sensor signals with chemiluminescence and acoustic signals.

It is interesting to speculate about the scaling of this work to larger or smaller combustors as the absorption sensor signal scales with the LOS path length. The work here illustrates that an atmospheric-pressure combustor with a 10-cm path has sufficient signal strength for successful use of either sensor and illustrates that the SNR of the 1.4-μm WMS-2f sensor is excellent even in liquid-fueled flames. The scaling of the WMS-2f 1.4-μm signals to smaller combustors depends primarily on the scaling of the noise, because we have previously demonstrated that WMS-2f detection limits three orders of magnitude smaller than the signals from this experiment. Larger combustors with longer path lengths will have larger signals, and for combustors larger than a 1-m LOS path length, one might wish to select weaker absorption transitions. Given the plethora of water vapor transitions in this region, we expect this is not a limitation, although research to select and characterize the optimum absorption transitions would be needed.

V. Conclusions

Two TDL sensors previously developed for nonintrusive gas temperature measurements have been compared for gas- and liquid-fueled, swirl-stabilized flames, providing the first demonstration of TDL thermometry in these practical flames. Both sensors are based on a single-laser two-line ratio concept, which significantly simplifies the sensor hardware. The scanned WMS-2f architecture offers several improvements over the wavelength-scanned, direct-absorption design, enabling a real-time temperature readout rate of 2 kHz and superior performance in environments with low-frequency flowfield noise that is a result of scattering from liquid droplets and soot particles. This sensor has the potential for detection of incipient lean blow out and, hence, for combustion control, enabling safe flame operation at a reduced fuel–air equivalence ratio.

Acknowledgments

We gratefully acknowledge support from the Office of Naval Research via the University of Cincinnati and the Global Climate Energy Program at Stanford.

References

[1] Hanson, R. K., and Jeffries, J. B., "Diode Laser Sensors for Ground Testing," AIAA Paper 2006-3441, June 2006.

[2] Furlong, E. R., Baer, D. S., and Hanson, R. K., "Real-Time Adaptive Combustion Control Using Diode-Laser Absorption Sensors," *Proceedings of the Combustion Institute*, Vol. 28, Combustion Inst., Pittsburgh, PA, 1998, pp. 103–111.

[3] Ebert, V., Fernholz, T., Giesemann, C., Pitz, H., Teichert, H., Wolfrum, J., Jaritz, H., "Simultaneous Diode-Laser-Based in Situ Detection of Multiple Species and Temperature in a Gas-Fired Power Plant," *Proceedings of the Combustion Institute*, Vol. 28, Combustion Inst., Pittsburgh, PA, 2000, pp. 423–430.

[4] Teichert, H., Fernholz, T., and Ebert, V., "Simultaneous in Situ Measurement of CO, H_2O, and Gas Temperatures in a Full-Sized Coal-Fired Power Plant by Near-Infrared Diode Lasers," *Applied Optics*, Vol. 42, No. 12, 2003, pp. 2043–2051.

[5] Sanders, S. T., Baldwin, J. A., Jenkins, T. P., Baer, D. S., and Hanson, R. K., "Diode-Laser Sensor for Monitoring Multiple Combustion Parameters in Pulse Detonation Engines," *Proceedings of the Combustion Institute*, Vol. 28, Combustion Inst., Pittsburgh, PA, 2000, pp. 587–593.

[6] Rieker, G. B., Li, H., Liu, X., Liu, J. T. C., Jeffries, J. B., Hanson, R. K., Allen, M. G., Wehe, S. D., Mulhall, P. A., Kindle, H. S., Kakuho, A., Sholes, K. R., Matsuura, T., Takatani, S., "Rapid Measurements of Temperature and H2O Concentration in IC Engines with a Spark Plug-Mounted Diode Laser Sensor," *Proceedings of the Combustion Institute* (to be published).

[7] Mattison, D. W., Jeffries, J. B., Hanson, R. K., Steeper, R. R., DeZilwa, S., Dec, J. E., Sjoberg, M., and Hwang, W., "In-Cylinder Gas Temperature and Water Concentration Measurements in HCCI Engines Using a Multiplexed-Wavelength Diode-Laser System: Sensor Development and Initial Demonstration," *Proceedings of the Combustion Institute* (to be published).

[8] Liu, J. T. C., Rieker, G. B., Jeffries, J. B., Hanson, R. K., Gruber, M. R., Carter, C. D., and Mathur, T., "Near-Infrared Diode Laser Absorption Diagnostics for Temperature and Water Vapor in a Scramjet Combustor," *Applied Optics*, Vol. 44, No. 31, 2005, pp. 6701–6711.

[9] Arroyo, M. P., and Hanson, R. K., "Absorption Measurements of Water Vapor Concentration, Temperature and Line Shape Parameters Using a Tunable InGaAsp Diode Laser," *Applied Optics*, Vol. 32, No. 30, 1993, pp. 6104–6116.

[10] Gharavi, M., and Buckley, S. G., "Single Diode Laser Sensor for Wide-Range H_2O Temperature Measurements," *Applied Spectroscopy*, Vol. 58, No. 4, 2004, pp. 468–473.

[11] Zhou, X., Liu, X., Jeffries, J. B., and Hanson, R. K., "Development of a Sensor for Temperature and Water Vapor Concentration in Combustion Gases Using a Single Tunable Diode Laser," *Measurement Science and Technology*, Vol. 14, No. 8, 2003, pp. 1459–1468.

[12] Zhou, X., Jeffries, J. B., and Hanson, R. K., "Development of a Fast Temperature Sensor for Combustion Gases Using a Tunable Diode Laser," *Applied Physics, B: Lasers and Optics*, Vol. 81, No. 5, 2005, pp. 711–722.

[13] Zhou, X., Liu, X., Jeffries, J. B., and Hanson, R. K., "Selection of NIR Water Vapor Transitions for In-Cylinder Measurement of Temperature During the Compression Stroke of an IC-Engine," *Measurement Science and Technology*, Vol. 16, No. 12, 2005, pp. 2437–2445.

[14] Zhou, X., Liu, X., Jeffries, J. B., Hanson, R. K., Li, G., and Gutmark, E. J., "Fast Temperature Sensor for Combustion Control Using H_2O Diode Laser Absorption Near 1.4 μm," AIAA Paper 2005-627, Jan. 2005.

[15] Reid, J., and Labrie, D., "Second-Harmonic Detection with Tunable Diode Lasers- Comparison of Experiment and Theory," *Applied Physics, B: Lasers and Optics*, Vol. 26, No. 3, 1981, pp. 203–210.

[16] Philippe, L. C., and Hanson, R. K., "Laser Diode Wavelength Modulation Spectroscopy for Simultaneous Measurement of Temperature, Pressure, and Velocity in Shock-Heated Oxygen Flows," *Applied Optics*, Vol. 32, No. 30, 1993, pp. 6090–6103.

[17] Liu, J. T. C., Jeffries, J. B., and Hanson, R. K., "Wavelength Modulation Absorption Spectroscopy with 2F Detection Using Multiplexed Diode Lasers for Rapid Temperature Measurements in Gaseous Flows," *Applied Physics B (Lasers and Optics)*Vol. 78, No. 3/4, 2004, pp. 503–511.

[18] Hovde, D. C., Hodges, J. T., Scace, G. E., and Silver, J. A., "Wavelength-Modulation Laser Hygrometer for Ultrasensitive Detection of Water Vapor in Semiconductor Gases," *Applied Optics*, Vol. 40, No. 6, 2001, pp. 829–839.

[19] Li, G., and Gutmark, E. J., "Combustion Characteristics of a Multiple Swirl Combustor," AIAA Paper 2003-0489, Jan. 2003.

[20] Li, H., Zhou, X., Jeffries, J. B., and Hanson, R. K., "Active Control of Lean Blowout in a Swirl-Stabilized Combustor Using a Tunable Diode Laser," *Proceedings of the Combustion Institute* (to be published).

[21] Li, H., Zhou, X., Jeffries, J. B., and Hanson, R. K., "Sensing and Control of Combustion Instabilities in Swirl-Stabilized Combustors Using a Diode Laser," AIAA Paper 2006-4395, July 2006.

[22] Rothman, L. S., Jacquemart, D., Barbe, A., Benner, D. C., Birk, M., Brown, L. R., Carleer, M. R., Chackerian, C. Jr., Chance, K., Coudert, L. H., Dana, V., Devi, V. M., Flaud, J-M., Gamache, R. R., Goldman, A., Hartmann, J-M., Jucks, K. W., Maki, A. G., Mandin, J-Y., Massie, S. T., Orphal, J., Perrin, A., Rinsland, C. P., Smith, M. A. H., Tennyson, J., Tolchenov, R. N., Toth, R. A., Vander Auwera, J., Varanasi, P., and Wagner, G., "The HITRAN Molecular Spectroscopic Database," *Journal of Quantitative Spectroscopy and Radiative Transfer*, Vol. 96, No. 2, 2005, pp. 130–204.

N. Clemens
Associate Editor